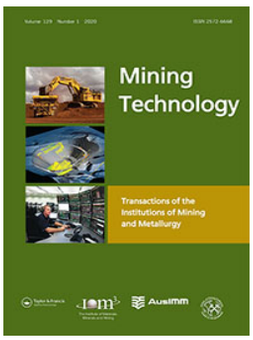

Taylor & Francis
Taylor & Francis Group

Mining Technology

Transactions of the Institutions of Mining and Metallurgy

ISSN: 2572-6668 (Print) 2572-6676 (Online) Journal homepage: https://www.tandfonline.com/loi/ymnt21

Stability assessment of underground mine stopes subjected to stress relaxation

Amoussou Coffi Adoko, Javier Vallejos & Robert Trueman

To cite this article: Amoussou Coffi Adoko, Javier Vallejos & Robert Trueman (2020) Stability assessment of underground mine stopes subjected to stress relaxation, Mining Technology, 129:1, 30-39, DOI: 10.1080/25726668.2020.1721995

To link to this article: https://doi.org/10.1080/25726668.2020.1721995

Published online: 04 Feb 2020.

MINING TECHNOLOGY
2020, VOL. 129, NO. 1, 30–39
https://doi.org/10.1080/25726668.2020.1721995

Stability assessment of underground mine stopes subjected to stress relaxation

Amoussou Coffi Adoko [a], Javier Vallejos[b] and Robert Trueman[a]

[a]School of Mining & Geosciences, Nazarbayev University, Astana, Republic of Kazakhstan; [b]Department of Mining Engineering, Advanced Mining Technology Center, Faculty of Physical and Mathematical Sciences, University of Chile, Santiago, Chile

ABSTRACT

Stress relaxation plays an important role in the design of underground stopes. The aim of this paper is to assess the stope stability in connection with the stress relaxation using a classification approach. Three types of stress relaxation were clearly defined, namely partial relaxation, tangential relaxation and full relaxation. A neural network classifier was implemented to assess the stability of the stopes on the basis of case histories of stope performances. The results of the classification were compared to existing empirical methods of quantifying the stress relaxation. Overall, the present study shows higher classification accuracies, especially when the stress relaxation was considered. The results suggested that the relaxation type can be a good predictor of stability. Relaxed stope (full and tangential stress relaxation) cases are the most critical in the sense that lower accuracies were obtained and the probability of correct classification is rather erratic.

ARTICLE HISTORY
Received 12 August 2019
Revised 19 January 2020
Accepted 21 January 2020

KEYWORDS
Stress relaxation; mine stope stability; neural network classifier; Mathew's stability graph

Introduction

The stress relaxation of a rock mass is a time-dependent phenomenon defined as the decrease of stress at a constant strain resulting in the deformation or weakening of the rock mass over time (Hudson and Harrison 1997). Paraskevopoulou et al. (2017) observed three stages of stress relaxation in brittle rocks based on laboratory testing. The first stage of stress relaxation corresponds to the phase where relaxation occurs with a decreasing rate; usually most of the relaxation takes place (55–95% of the total stress relaxation) during the first stage. In the second stage, the stress decreases at a constant rate and in the third stage, no further stress relaxation takes place. Field observations also show this time-dependent behaviour in the rock mass especially surrounding underground openings (Kaiser et al. 2001). In general, the rock mass is subjected to stress and strain changes after excavation, influencing the long-term behaviour of the rock and the properties of the damage zone. In underground hard rock mines, relaxation is best described as a loss of confinement and occurs when the compressive stress is absent in the vicinity of and in a direction parallel to the surface of an excavation wall or roof due to subsequent mining of nearby stopes (Diederichs 2003). It is a key controlling factor in the stability of a mine stope and the interacting openings especially with complex geometries (Diederichs and Kaiser 1999). This controlling factor of the stress relaxation on excavation stability has been recognized by several researchers (Kaiser et al. 1997; Diederichs and Kaiser 1999; Kaiser et al. 2001; Suorineni et al. 2001; Stewart and Trueman 2004). A parametric study carried out by Suorineni et al. (2001) indicated that the stress relaxation has unfavourable effects on stope stability when the induced stress is less than a critical value.

In the design of underground hard rock mines with an open stoping mining method, the Mathew's stability graph method is well accepted and widely used around the world today due to its simplicity and potential flexibility to accommodate a wide range of hard rock mining methods. One of the limitations of the method however, is its inappropriateness for low compressive stresses and tensile stresses in excavation faces. These types of stresses often occur along the hangingwalls and footwalls of relatively tall stopes created, for example, in longhole open-stoping, AVOCA or other similar method. However, assessing the stability of underground stopes using the stability graph method chart is more appropriate for certain types of in-situ stress conditions. It has been shown that the method usually yields reliable results especially in instances where the maximum induced tangential stress provides enough compressive stress to confine the excavation faces, but the method does not account properly for relaxation situations (Mitri et al. 2011). Therefore, several studies in which an adjustment of the stress factor (A) in the stability graph method, were proposed. Stewart and Trueman (2004) found that tangential relaxation and full relaxation have the most adverse effect on excavation stability compared to partial relaxation and accordingly they proposed an adjustment of the

CONTACT Amoussou Coffi Adoko amoussou.adoko@nu.edu.kz; aadoko2004@yahoo.fr School of Mining & Geosciences, Nazarbayev University, Astana 010000, Republic of Kazakhstan

stress factor in the extended Mathews stability. Similarly, Mitri et al. (2011) proposed adjustments in the rock stress factor by introducing a penalty to reflect the effect of low-stress or tensile stress on critical face stability as an attempt to overcome that fundamental limitation in the stability graph method. Meanwhile, some studies suggest that the effect of the stress relaxation on excavation stability is not significant (Potvin 1988; Milne et al. 2002). This may be due to the fact the phenomenon of relaxation and rheology behaviour of hard rock and the relations between the various time-dependent behaviours appear to be complex and not fully investigated yet, compared with those on soft rock (Hashiba and Fukui 2016; Yang et al. 2017).

For these reasons, it is important to determine the extent of the effect of the types of stress on stope stability and to make a few suggestions as alternatives or complements to the use of the stability graph method. Hence, in this paper, a classification model for stope stability constrained by the relaxation types is implemented. The classification approach is justified by the fact that in a previous study by Stewart and Trueman (2004), a misclassification of failed stopes was used to account for the relaxation effect. An artificial neural network (ANN)-based classifier is chosen as a convenient tool to recognize the effect of relaxation.

Methods

ANN-based classifiers

ANNs are known as artificial intelligence tools which model human brain functions and learn from sample data presented to them. They are used to capture the relationship among data such as correlations, patterns or clusters. ANNs consist of neurons which are the basic processing units; they are densely interconnected in such a way that performing large parallel computations is possible. Theories on ANNs are widely available in the literature. They can fairly approximate any kind of function and also be used as a classifier (Engelbrecht 2007). Readers may refer to Veelenturf (1995) for theoretical background while a concise overview on the subject can be found in Adoko et al. (2013). According to the network architecture or the training algorithm, the types of ANN include back-propagation, counter-propagation, feed-forward and dynamic networks. They can also be classified as static (feed-forward) or dynamic. In each neuron n input data are processed and a single output is determined as follows:

$$y = f\left(\sum_{i=1}^{n} w_i x_i + \theta\right) \tag{1}$$

where x_i,w_i,θ and f are the values of the ith input, the values of the ith weight, the bias of the neuron and the activation function of the neuron, respectively (Veelenturf 1995). A network consists of at least three layers of neurons (input, hidden and output layer) as illustrated in Figure 1. The first one, the input layer distributes the input dataset. It should be noted that there is no processing in that layer; each neuron receive just one component of the input vector which gets distributed, unchanged, to all neurons from the input layer. The last layer is the output layer which outputs the processed data. The layers between the input one and the output one are called hidden layers. In feed-forward neural networks (FFNNs), there are no feedback elements; inputs are received and simply forwarded through all the next layers to obtain the outputs. As an illustration of how the output is computed, the outputs of the second hidden layer J_2 (Figure 1) are calculated explicitly as follows:

$$Y_k^{J_2} = f_2\left(\sum_{j=1}^{N_1} w_{k,j}^2 f_1\left(\sum_{i=1}^{N_0} w_{j,i}^1 x_i + \theta_j^1\right) + \theta_k^2\right) \tag{2}$$
$$k = 1, 2, \ldots, N_2$$

where N_0, N_1 and N_2 are the number of inputs, neurons in the first layer, and neurons in the second layer; $Y_k^{J_2}$ is the kth output of J_2; f_2 is the activation function of J_2;$w_{k,j}^2$ is the weight between the kth neuron of J_2 layer and the jth neuron of J_1 layer; f_1 is the activation function of the first layer; $w_{j,i}^1$ is the weight between the jth neuron of the first layer and ith input; x_i is the ith input; θ_j^1 is the bias of jth neuron in the first layer and θ_k^2 is the bias of kth neuron in the second layer. Given a pair of training datasets and its corresponding target values, the network computes the outputs (according to Equation (2)) using its initial weights and biases. Then, the weights and biases are adjusted by comparing the output values and the target values, until the network outputs match the targets. Usually, in the training process, the sum of squared errors is used as a performance index while the Levenberg-Marquardt algorithm (back-propagation) or any variant is mostly implemented to minimize the errors (Adoko et al. 2013).

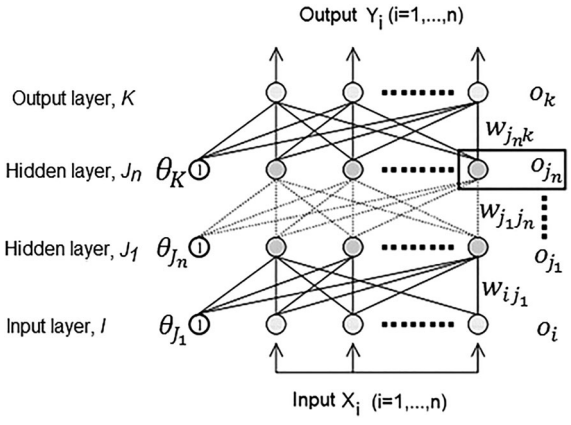

Figure 1. FFNN schematic diagram.

When FFNNs are used as a classifier, several structures can be employed depending on the classification of the feature patterns including the one-against-all, weighted one-against-all, binary coded, parallel-structured, weighted parallel-structured and tree-structured (Lam et al. 2014). For all these classifiers, the input pattern of$x(k) = \{x_1(k), x_2(k), \ldots, x_n(k)\}$ is recognized as the feature vector of a target object to be classified. Basically, these classifiers group the feature patterns into N classes using a supervised learning framework. For example, in the one-against-all classifier, a multiple-input-single-output fully connected FFNN correlates the feature pattern **x**(k) in the form of input and generates a single value $y(k)$ as output. Then, the target output yd(k) takes value of i whenever the input feature pattern **x**(k) corresponds to the class i. Hence, this classifier is trained in such as a way that the output $y(k)$ is in the maximum proximity to yd(k) in accordance with the class, which the feature pattern **x**(k) belongs to. The output class j is generically represented by the equation as follows:

$$j = \arg\min_i \{|y(k) - i|, i \in \{1, \ldots N\}\} \quad (3)$$

where $|\cdot|$ symbolizes the absolute value operator.

A brief review of the stability graph method

The stability graph commonly known as the Mathews stability chart method has its origin from a project investigating stope stability in deep Canadian mines (Mathews et al. 1981). Since then, several authors have elaborated on the method and expanded the initial database from 26 case histories to more than 400 case histories collected from mines in North America, Australia, Chile and England (Potvin 1988; Mawdesley et al. 2001; Vallejos et al. 2016) with a series of modifications to the way the stability number and its factors are determined. The stability graph relates the size of an excavation surface to the rock mass competency to provide an indication of stability or instability. It involves two main parameters: the stability number, (N) and the hydraulic radius (HR). The stability number N is defined as follows:

$$N = Q' \times A \times B \times C \quad (4)$$

$$Q' = \frac{RQD}{J_n} \times \frac{J_r}{J_a} \quad (5)$$

In Equations (4) and (5), A is the rock stress factor, B is the joint orientation adjustment factor and C is the gravity adjustment; Q' represents the rock mass quality determined by the rock quality designation (RQD), the joint set number (J_n), the joint roughness number (J_r) and the joint alteration number (J_a). Meanwhile HR is defined as the ratio of a stope face area over its perimeter. The adjustment factors are determined using charts as provided in Figure 2(a–c).

Relaxed stope surface data description

The relaxation case histories utilized for this study, came from several sources across the world pertaining to open stoping mining environments. The dataset was compiled from relevant literature and the contributing mines included Ruttan mine (Pakalnis 1986; Potvin 1988), Detour Lake mine (Pakalnis et al. 1991), South Crofty mine (Stewart 2005), Cobar mine (Mathews et al. 1981) and Kundana Gold mine (Stewart 2005). Three types of stress relaxation have been considered according to the magnitude and direction of the principal stresses obtained from 3D modelling using Map3D (Stewart and Trueman 2004; Stewart 2005). Partial relaxation of stope surfaces refers to a situation where σ3 is less than 0·2 MPa, while σ2 and σ1 both exceed 0·2 MPa. Full relaxation is defined as stope surfaces where σ3 and σ2 are both less than 0·2 MPa. Tangential relaxation is defined as stope surfaces where at least one of the modelled principal stresses is less than 0·2 MPa and the corresponding direction of the stress deviates less than 20° parallel to the excavation wall in a 3D situation; this means the angle between the stress direction and the stope surface dip or strike is less than 20°. It is noted that based on these definitions, a stope surface can be simultaneously fully relaxed and tangentially relaxed. When evaluating the potential for stress relaxation, the choice of three-dimensional modelling will impact upon the modelled state of relaxation. For some stope geometries, a two dimensional stress analysis will predict that the rock mass in the vicinity of an excavation is relaxed, but it may not be when a three-dimensional stress analysis is performed. In such a case, the stope surface will not be truly relaxed. Hence, the results of this study are constrained by the assumption of 3D linear elastic modelling of Map3D software which had been used to estimate the in-situ stress (Stewart and Trueman 2004).

The dataset consists of key information on factors influencing the stope performance including the stope geometry, geological properties, modelled in-situ stress, and the stope response (stable, failure and major failure). The input parameters are namely, the hydraulic radius HR, rock quality designation RQD, joint set number Jn, joint roughness number Jr, joint alteration number Ja, stress factor A, joint orientation adjustment factor B, gravity factor C, and the stress relaxation category. The output is the stope performance (stability) which is being evaluated in this study. For the purpose of classifying the stope responses, they were categorized into three classes: stable, failed and major failure. Figure 3 shows histograms of the two main parameters of the ANN model.

The dataset is composed of 43%, 31.3%, and 25.7% of stable, failed and major failure, respectively. Also, 23.7%, 31.3% and 45 29% correspond to fully relaxed, tangentially and partially relaxed cases, respectively.

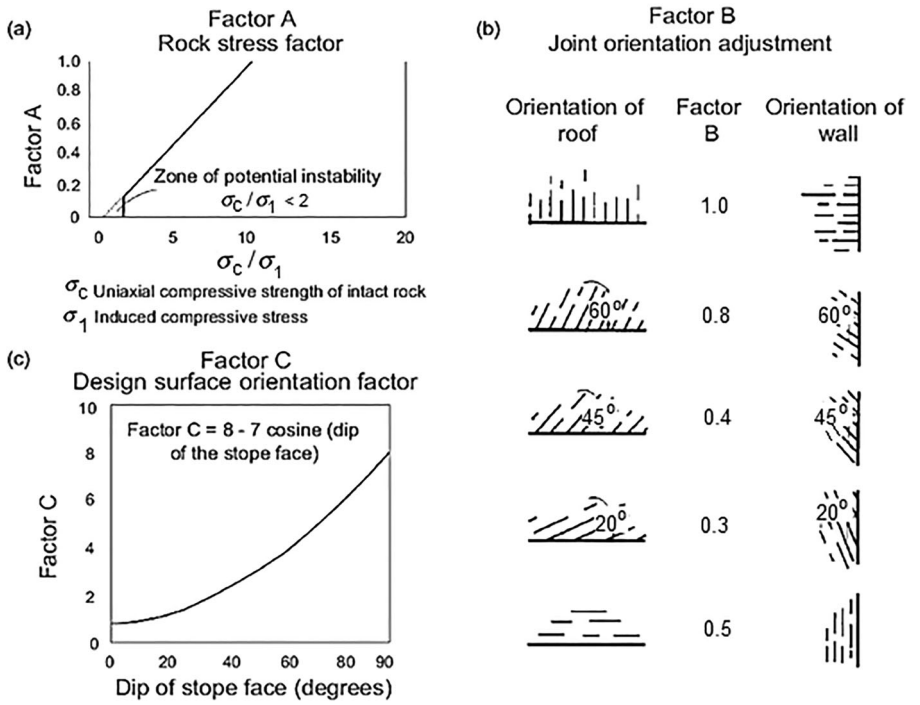

Figure 2. Adjustment factors of the stability graph (Vallejos et al. 2016).

A statistical description of the data and a sample of the data are provided in Table 1 while a stability graph of the dataset is shown in Figure 4. For the purpose of implementing the ANN-based classifier, it was necessary to translate the relaxation type variable into a numerical attribute using a semi-quantitative encoding (Adoko et al. 2017).

Results of the ANN classification

In order to account for the effect of the stress relaxation on the ANN-classifier's ability to recognize the stope stability, several data structures were used. First, the entire dataset was employed with $A = 1$ for each case history representing situations where no adjustment due to relaxation in the Mathews stability graph was considered; then the stability numbers were recalculated according to (Stewart and Trueman 2004), i.e. $A = 0.7$ for relaxed stopes and $A = 1$ for partially relaxed. Next, the classification modelling was conducted according to each type of relaxation. For most cases, the dataset was randomly divided into three parts: training (70%), validation (15%) and testing (15%). The inputs consist of three parameters namely, the HR, N and the relaxation category. The output consists of the following vectors(1, 0, 0); (0, 1, 0) and(0, 0, 1) representing stable stope walls, failed stope walls and major failure of stope walls, respectively. These vectors were used because the target data for pattern recognition networks should consist of vectors of all zero values except for a 1 in element *i*, where *i* is the class they are to represent. Several FFNNs were attempted in order to classify the stope stability. Three principal steps were involved: defining the network, then the training and testing of the network. The required computation was carried out using the neural network toolbox of MATLAB software (version R2014a). It was important to determine the optimum network architecture to achieve reliable results. After a series of experiments based on the trial-and-error method (with 1–4 hidden layers and 10–60 neurons in each), a maximum of two hidden layers in the FFNN were found suitable for most cases. The cross-entropy algorithm was used to evaluate the performance of the network. The transfer functions logistic sigmoid (Logsig) in the hidden layers and softmax

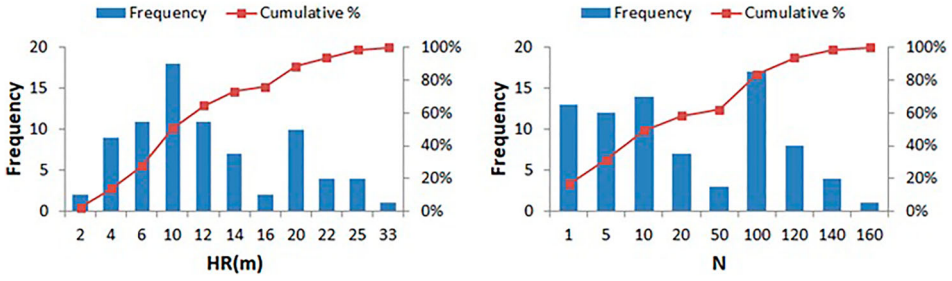

Figure 3. Histogram of the dataset corresponding to HR and *N* parameters. Images are available in colour online.

Table 1. Statistical description of the dataset.

	Q'	A	B	C	N	HR	σ_c/σ_i	σ1	σ2	σ3	Relaxation	Stability
Unit	–	–	–	–	–	–	–	MPa	MPa	MPa	Logic	Logic
Max	60.0	1.0	0.5	8.0	154.6	33.0	6846.2	21.0	14.0	0.4	3	Major failure
Min	0.3	0.7	0.5	3.7	0.6	2.0	−2966.7	0.0	−7.5	−7.1	1	Stable
Mean	14.3	0.9	0.5	6.0	38.0	11.0	−56.0	6.3	2.0	−0.7	N/A	N/A
St.dev.	16.6	0.1	0.0	1.2	43.6	6.2	1082.1	5.7	3.7	1.4	N/A	N/A

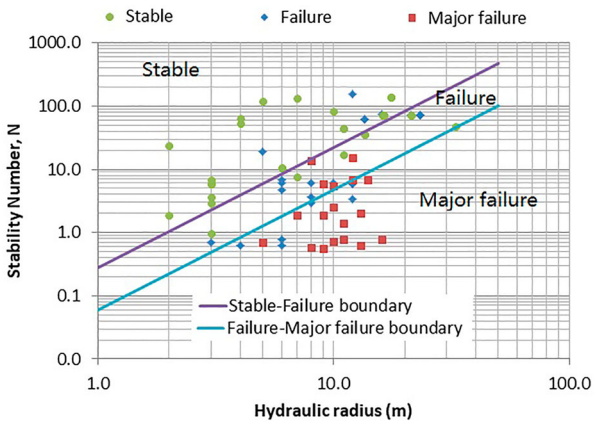

Figure 4. Stability graph of the dataset used in this study. Images are available in colour online.

transfer function in the output layer were used according to:

$$\log sig(n) = \frac{1}{1+e^{-n}} \tag{6}$$

$$soft\ \max(n) = \frac{e^n}{\sum e^n} \tag{7}$$

These transfer functions return values within [0, 1] which makes them convenient for classification problems and the main advantage of using *softmax* is that it represents also the output probabilities range for having any stope classified as stable, failed or with major failure.

The results of the classification are shown in Figures 5–7. Figure 5(A and B) compare the classifier network performances without and with the consideration of the relaxation effect, respectively. As it can be seen, higher performance was achieved when the type of stress relaxation was specified in the input dataset. This indicates that the implemented network recognizes better the stope wall stability constrained by stress relaxation and the relaxation is highly correlated to the stope response.

A confusion matrix of the classification corresponding to the whole dataset with relaxation was obtained and shown in Figure 6. This figure illustrates the classifiers' predictive performance. As it can be seen, the confusion value (i.e. fraction of samples misclassified) for training, validation, testing and all datasets together is 8.9%, 25%, 16.7% and 12.5%, respectively, which is considered very high. The target classes are the actual classes and the output classes are the predicted classes. Figure 6 shows that overall, two cases of stable stope were misclassified as failed while three cases were misclassified the other way around; three cases of major failure of stope were misclassified as failed stope (minor failure).

In addition, the receiver operating characteristic (ROC) and the quality of the classification (accuracy, sensitivity and specificity) were employed to further assess the performance of the classification. The following indices (accuracy, sensitivity and specificity) defined (in Equations (8)–(10)) were calculated and are provided in Table 2.

$$\text{Accuracy} = \frac{T_p + T_n}{T_p + T_n + F_p + F_n} \tag{8}$$

$$\text{Sensitivity} = \frac{T_p}{T_p + F_n} \tag{9}$$

$$\text{Specificity} = \frac{T_n}{T_n + F_p} \tag{10}$$

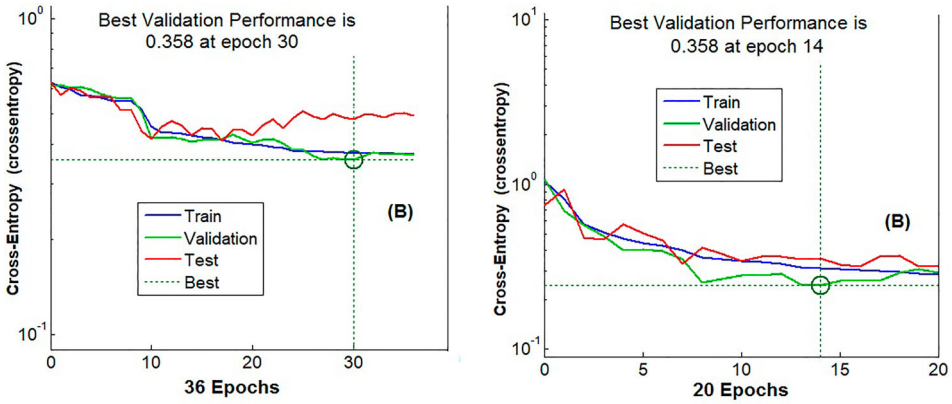

Figure 5. ANN-based classifier performance: (A) without relaxation effect; (B) with relaxation effect. Images are available in colour online.

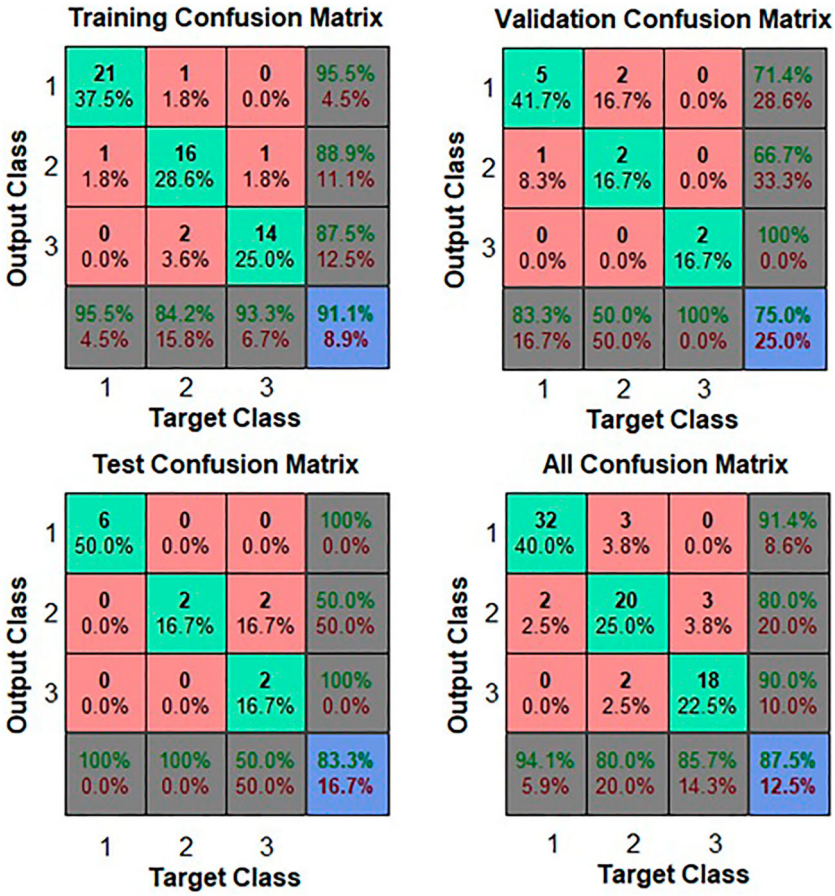

Figure 6. Confusion matrix of the classification. Images are available in colour online.

T_p, T_n, F_p and F_n stand for true positive, true negative, false positive and false negative, respectively.

The ROC is an indicator commonly used to check the quality of classifiers. Figure 7 shows the ROC curves for the entire dataset. For each class, the ROC uses a threshold to the outputs in order to recognize the class to be predicted (Qi et al. 2018). Two values are calculated namely, the true positive rates and the false positive rates. The closer the ROC curves to the upper left corner, the better the classification. In Figures 6 and 7, classes 1, 2 and 3 stand for stable stope, failed stope and major failure of stopes, respectively. The results indicate that class 2 is far from the upper left corner compared to the other classes. This means class 2 is not very well classified. This is in agreement with Table 2 where it can be seen the sensitivity of class 2 (failure) is 80%. The FFNN-classifier never misclassified a stable stope as a major failure and vice versa. Table 2 summarizes the indices of performance for each class. The last rows of Table 2 show the classification results according to the methodology of Stewart and Trueman (2004) where a logistic regression model is used to determine the boundary of stable and unstable zones of the stability graph (see Figure 4) with the assumption of $A = 0.7$ for relaxed stopes and $A = 1$ for partially relaxed.

It should be noted that because of the limited dataset, full and tangential relaxation cases were modelled together. Overall, from Table 2, it can be seen that the neural network classifier outperformed previous results. In particular, in partial relaxation conditions, the network can be classified with very high accuracy, sensitivity and specificity (all above 90%). However, when the stopes are fully and tangentially relaxed, the

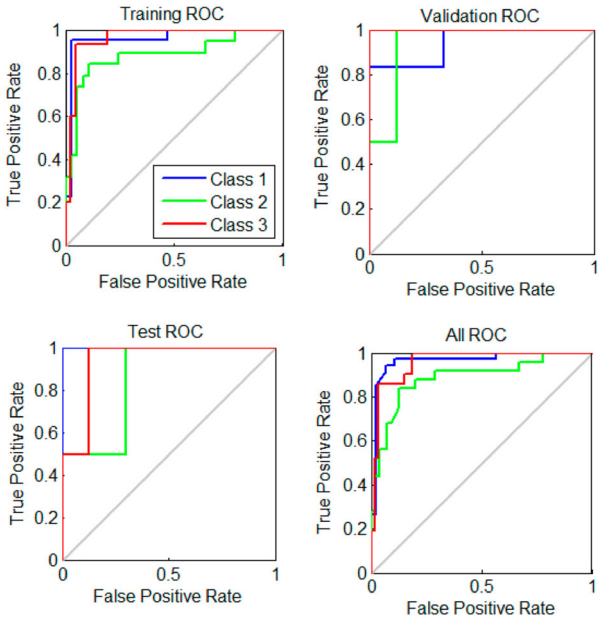

Figure 7. ROC curves for the classification. Images are available in colour online.

Table 2. Summary of the classification performance.

	Excavation stability	Accuracy	Sensitivity	Specificity	Confusion value
Whole dataset ($A = 1$)	Stable	0.88	0.88	0.87	0.27
	Failure	0.74	0.48	0.85	
	Major failure	0.86	0.81	0.88	
	Average	0.83	0.72	0.87	
Whole dataset (with relaxation)	Stable	0.94	0.94	0.93	0.12
	Failure	0.88	0.80	0.91	
	Major failure	0.94	0.86	0.97	
	Average	0.92	0.87	0.94	
Full and tangentially relaxed	Stable	0.91	0.96	0.85	0.11
	Failure	0.91	0.77	0.97	
	Major failure	0.95	0.86	0.97	
	Average	0.92	0.86	0.93	
Partial relaxation	Stable	0.97	0.90	1.00	0.083
	Failure	0.94	0.92	0.96	
	Major failure	0.92	0.93	0.91	
	Average	0.94	0.92	0.96	
(Stewart and Trueman 2004)	Stable	0.84	0.76	0.89	0.33
	Failure	0.66	0.52	0.73	
	Major failure	0.83	0.67	0.88	
	Average	0.78	0.65	0.83	

classification performance is a little poorer. The sensitivity for failed stopes is 77% which means the amount of false prediction is slightly higher (23%) but is still within an acceptable range compared to when $A = 0.7$ the false predictions for the failed stopes were 48%. In summary, although high accuracy was achieved in general, the results indicate that the FFNN-classifier cannot always recognize failed stopes (based on the false prediction), especially when full and tangential stress relaxation prevail.

In addition, 3D probability graphical representation (in X–Y view) of failed stopes is plotted with colour code and provided in Figure 6 using the nearest neighbour interpolation method. This figure provides a better visualization of the stability zones with their associated probabilities. They consist of areas of variable colours. Intuitively, a rough area corresponding to failed stope is delimited by two lines (just for illustration purposes) as shown in Figure 8(A and B). In both Figure 8(A and B), the area above represents the stable zone while the bottom area is where major failure of stopes will be located. In Figure 8(A), the yellow and light blue areas have high probability to be stable (with a probability of correct prediction more than 0.6) while in Figure 8(B) the yellow and light blue areas correspond to cases where a stope will probably fail. Nevertheless, it is more logical for the failed area on the graph to be irregular. It is noted that in Figure 8(A and B) and, reference is made in respect of stable stopes and failed stopes, respectively. Similarly, major failure in stopes could be considered as a reference as well.

Another important result of the study is the quantification of the effect of the type of relaxation on the excavation response. 3D probability graphical representation (in X–Y view) of stable stopes and major failure of stopes are plotted with colour code as shown in Figure 9(A and B). In these figures, the x-axis represents the relaxation type and y-axis HR. It was found that the relaxation type can substitute the stability number (N) as the goodness of fit (R^2) when fitting the data points of the graphs was higher than 0.86. As it can be seen in both figures, there was no major difference between full and tangential relaxations for both figures. However, partial relaxation is a good prediction of stability (correlates very well with the stope response). As a matter of fact, when

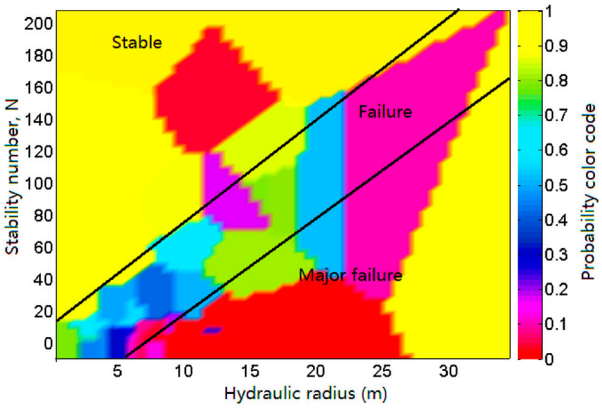

A Probability map of stable stopes

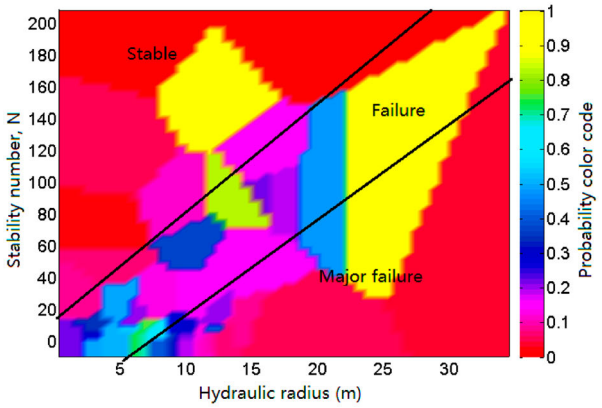

B Probability map of failed stopes

Figure 8. (A) Probability map of stable stopes. (B) Probability map of failed stopes. Images are available in colour online.

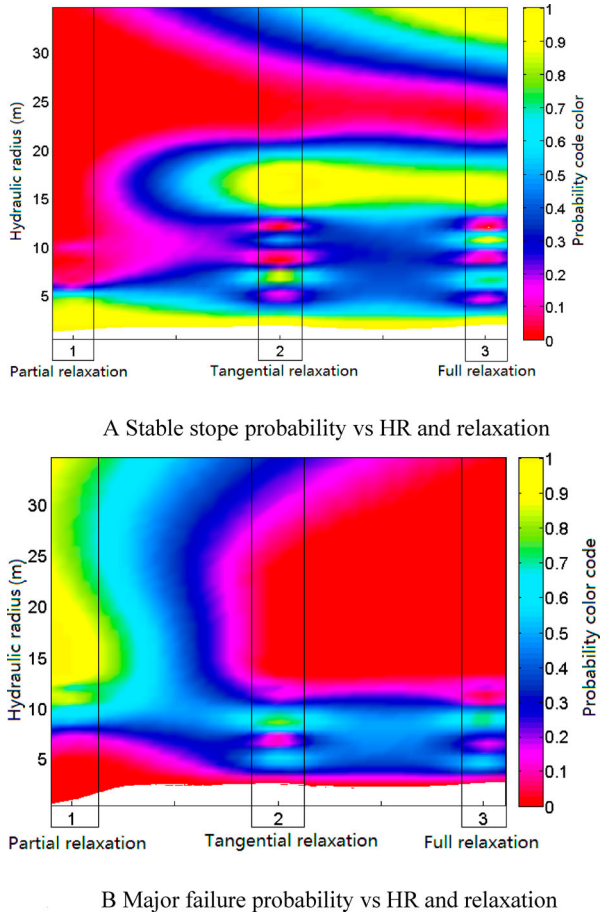

Figure 9. (A) Stable stope probability vs HR and relaxation. (B) Major failure probability vs HR and relaxation. Images are available in colour online.

HR<5 m, the stopes are likely to be stable with high probability (Figure 9(A)) and when HR>12 m, major failure are likely to occur in the stopes with high probability (Figure 9(B)). While major failure is less associated with full and tangential relaxations and stable stopes are found within a narrow range of HR between 15 and 20 m.

Comparison with existing results and discussions

The results of this study were compared to those of existing studies for discussion purposes. In order to make any meaningful comparison, the entire dataset was categorized into two classes: stable stopes on one hand and failed stopes on the other, similar to previous studies (Stewart and Trueman 2004). The performances of each method are summarized in Table 3. The sensitivity and specificity were determined (Equations (9) and (10)); the confusion value of the classification is basically the percentage of misclassifications. The classifications were carried out for each type of relaxation and the whole dataset using: a stress factor of $A = 1$ as in the stability graph (Potvin 1988); $A = 0.7$ for relaxed stopes and $A = 1$ for partially relaxed stope (Stewart and Trueman 2004); $A = 0.9\exp^{11(\sigma_t/UCS)}$ (Diederichs and Kaiser 1999) and the FFNN-based classifier. As it can be seen, the FFNN-based method yielded the least confusion value (3.7%) which is extremely low in comparison with that of existing work. In short, the proposed methodology showed improvement over previous studies.

In general, the results indicate good classification performance with the confusion values around 10% (see Table 2). An interpretation of this is that if new data (with the assumption that their statistical description is very close to that of the employed dataset), were presented to the network, there would be likely up to 1 or 2 misclassified stope stability out of 10 cases. This is quite reasonable based on the performances of the existing stability graphs (Potvin 1988; Clark 1998; Mawdesley et al. 2001; Vallejos et al. 2017).

The probability maps reflect peculiarities in the stability zones. For example, the red area in the left upper corner of Figure 8(A) and the yellow area on the right bottom corner Figure 8(B). The first area corresponds to failed stopes (see Figure 8(B)) while located into an area supposedly to be stable. This map is dictated by the data employed. The actual case history data corresponding to this area is stope '13D F/w' with $N = 154$, HR = 12 m, subjected to partial relaxation and pertained to the Ruttan mine (Pakalnis 1986). The stability graph would evaluate any new stope with similar data as stable but with the use of the probability maps of stability, the stope would be assessed as failed (very low probability of being stable, less than 0.1). However, this does not mean that any new stope from another mine falling

Table 3. Summary of the classification performance.

Factor A		Full relaxation	Tangential relaxation	Partial relaxation	Whole dataset
The stability graph ($A = 1$)	Sensitivity	0.90	0.86	0.90	0.88
	Specificity	0.67	0.64	0.92	0.80
	Confusion value	0.21	0.24	0.083	**0.17**
Stewart and Trueman (2004)	Sensitivity	0.70	0.71	0.90	0.76
	Specificity	0.88	0.82	0.92	0.89
	Confusion value	0.21	0.24	0.083	**0.16**
Diederichs and Kaiser (1999)	Sensitivity	0.70	0.71	0.90	0.76
	Specificity	1.0	0.91	0.92	0.93
	Confusion value	0.16	0.2	0.083	**0.13**
FFNN-based classification	Sensitivity	1.00	0.92	0.90	94.1
	Specificity	0.77	0.91	1.00	95
	Confusion value	0.10	0.08	0.02	**0.037**

within that area will necessarily fail. The probability of failure will be higher if the stope to be evaluated has similar characteristics (geology, design, etc …) as that of the stope '13D F/w'. Another example is the yellow area in the right bottom corner Figure 6(B). Using the stability graph, in principle a stope falling in that area would fail; nevertheless the actual case history data corresponding to this area shows stable stope walls. Therefore, it is necessary to make use of engineering judgment when dealing with empirical data. One advantage of these coloured coded maps is the visualization of the associated probability of the stope performance which is useful and more convenient for less experienced users.

As far as the relaxation maps are considered, the stability of the stopes is affected by the stress relaxation in different ways. The classification performances suggest that full and tangential relaxations are found to be critical in the sense that any stope stability under these types of relaxation will be predicted with lower accuracy while partial relaxation indicates failed stopes or major failure in stopes. In other words partial relaxation indicates more instability around the stopes which is in agreement with field observation. It is noted that tangential relaxation and full relaxation would have an adverse effect on excavation stability especially within a range of HR between 20 and 30 m approximately. Also, when the minor principal stress is negative (i.e. tensile) the intermediate principal stress has been identified as significantly affecting jointed rock mass behaviour as substantiated by most stope cases from the employed dataset.

In summary, these results are not only in agreement with existing studies but also complement them. With the use of the obtained colour coded maps, there is no need to determine specifically any boundary limit using logistic regression; and the stability of any stope can be determined in a probabilistic way. The relaxation map will be particularly relevant in a mining environment where rock mass properties (geotechnical domains) show limited variability i.e. N doesn't vary that much. However, this study has some limitations. For example the data range, size, dimension, variability dictate the accuracy and the reliability of the classification. There were limited case studies to investigate full and tangential stress relaxation separately; more data points would provide an additional insight to the individual effect of the tangential and the full relaxation stress. Also, concerning the FFNN-classifier, the results show poor performance in predicting failed stopes, further studies may focus on improving this. Nonetheless, the results of this study can serve as valuable inputs for further studies with focus on the improvement of the FFNN architecture or implementing other types of classifiers and redefining the thresholds used for the classification. Although the main idea behind the stability graph was to establish a non-rigorous method for open stope performance prediction (Stewart and Forsyth 1995), there has been an increasing need from the industry to develop more accurate and reliable tools. The results of this study could contribute toward improving the reliability of the existing graph with the implementation of FFNN-classifier as a complementary tool to existing stability graphs.

Conclusion

In this paper, an approach based on a neural network classifier model was implemented to assess the stability of underground mine stope walls where three types of stress relaxation namely, partial, full and tangential relaxation were defined. Historical cases of open stope design data were employed to establish the different models. The data included mainly the stability number N defining the rock mass properties, the hydraulic radius HR accounting for the stope geometry and stress relaxation category reflecting the design characteristics of the stopes. The output was the stope response which was categorized into three classes (stable, failure and major failure). A feed-forward network (FFNN) classifier with 2–3 hidden layers was implemented to recognize each type of stability classes. In general, the results indicated very good performances of the models. High accuracies were achieved (73–98%) for the different cases that were considered while the extended Mathews stability method showed 67%. These results indicated improvement over the existing methods. This indicates that the proposed classifier was extremely capable of differentiating clearly stable stope and stope with major failure.

Secondly, the probabilities of classifying correctly the stable and failed stopes were determined from the network outputs and were plotted against HR, N and the relaxation type in a 2D graph with colour code for visualization purposes. Overall, it is found that the stability zones were consistent with existing graphs but within a certain range of N and HR values. However, outside this range, some differences were observed. In addition, the results suggested that the relaxation type is also a good predictor of stability. However, relaxed stope (full and tangential stress relaxation) cases were the most 'critical' in the sense that lower accuracies were obtained and the probability of correct classification was rather erratic. Therefore, sound engineering judgment is required when dealing particularly with relaxed stope walls. One of the merits of the current study is that the probability map of having a stope stable, failed or with major failure can used to assess open stope stability. The map can be updated when more data become available. The results of this study could also contribute to the probabilistic design of mine stopes in general. Based on the results, it is suggested that the FFNN-based classifier could serve as alternative to the conventional stability graph method in the design of open stope especially in narrow-vein geometries which are often prone to stress relaxation effects.

Acknowledgment

The authors wish to acknowledge the contribution of the anonymous reviewers.

Disclosure statement

No potential conflict of interest was reported by the author(s).

Funding

This study was supported by the Faculty Development Competitive Research Grant program of Nazarbayev University, Grant N° 090118FD5338; and the Advanced Mining Technology Center (AMTC), University of Chile, through the Basal Project FB-0809.

ORCID

Amoussou Coffi Adoko http://orcid.org/0000-0003-1396-7811

References

Adoko A-C, Jiao Y-Y, Wu L, Wang H, Wang Z-H. 2013. Predicting tunnel convergence using multivariate adaptive regression spline and artificial neural network. Tunnel Underground Space Technol. 38(0):368–376.

Adoko AC, Phumaphi PT, Zvarivadza T. 2017. Quantifying rock mass behavior around underground excavations. The 51st US Rock Mechanics / Geomechanics Symposium, June 25–28; San Francisco, CA.

Clark LM. 1998. Minimizing dilution in open stope mining with a focus on stope design and narrow vein longhole blasting [MSc thesis]. Vancouver: University of British Columbia.

Diederichs MS. 2003. Manuel Rocha medal recipient rock fracture and collapse under low confinement conditions. Rock Mech Rock Eng. 36(5):339–381.

Diederichs MS, Kaiser PK. 1999. Tensile strength and abutment relaxation as failure control mechanisms in underground excavations. Int J Rock Mech Min Sci. 36(1):69–96.

Engelbrecht AP. 2007. Computational intelligence. Chichester: Wiley.

Hashiba K, Fukui K. 2016. Time-dependent behaviors of granite: loading-rate dependence, creep, and relaxation. Rock Mech Rock Eng. 49(7):2569–2580.

Hudson JA, Harrison JP. 1997. 13 - Rock dynamics and time-dependent aspects. In: Hudson JA, Harrison JP, editors. Engineering rock mechanics. Oxford: Pergamon; p. 207–221.

Kaiser PK, Falmagne V, Suorineni FT, Diederichs MS, Tannant DD. 1997. Incorporation of rock mass relaxation and degradation into empirical stope design. The 99th CIM Annual General Meeting; Vancouver, Canada.

Kaiser PK, Yazici S, Maloney S. 2001. Mining-induced stress change and consequences of stress path on excavation stability — a case study. Int J Rock Mech Min Sci. 38 (2):167–180.

Lam HK, Ekong U, Liu H, Xiao B, Araujo H, Ling SH, Chan KY. 2014. A study of neural-network-based classifiers for material classification. Neurocomputing. 144:367–377.

Mathews K, Hoek E, Wyllie D, Stewart S. 1981. Prediction of stable excavation spans at depths below 1000 m in hard rock mines. CANMET Report, DSS Serial No OSQ80-00081.

Mawdesley C, Trueman R, Whiten WJ. 2001. Extending the Mathews stability graph for open–stope design. Min Technol. 110(1):27–39.

Milne D, Yao M, Allen G. 2002. Quantifying the effect of hanging wall undercutting on stope dilution. The 104th CIM annual general meeting, Vancouver.

Mitri HS, Hughes R, Zhang Y. 2011. New rock stress factor for the stability graph method. Int J Rock Mech Min Sci. 48(1):141–145.

Pakalnis RT. 1986. Empirical stope design at the Ruttan Mine, Sherritt Gordon Mines Ltd [PhD dissertation]. Vancouver: University of British Columbia.

Pakalnis RT, Tenney D, Lang B. 1991. Numerical modelling as a tool in stope design. CIM Bull. 84:64–73.

Paraskevopoulou C, Perras M, Diederichs M, Amann F, Löw S, Lam T, Jensen M. 2017. The three stages of stress relaxation - observations for the time-dependent behaviour of brittle rocks based on laboratory testing. Eng Geol. 216:56–75.

Potvin Y. 1988. Empirical open stope design in Canada [PhD dissertation]. The University of British Columbia.

Qi C, Fourie A, Ma G, Tang X. 2018. A hybrid method for improved stability prediction in construction projects: a case study of stope hangingwall stability. Appl Soft Comput. 71:649–658.

Stewart PC. 2005. Minimising dilution in narrow vein mines [PhD dissertation]. Queensland: The University of Queensland.

Stewart SBV, Forsyth WW. 1995. The Mathews method for open stope design. CIM Bull. 88(992):45–53.

Stewart PC, Trueman R. 2004. Quantifying the effect of stress relaxation on excavation stability. Min Technol. 113 (2):107–117.

Suorineni FT, Tannant DD, Kaiser PK, Dusseault MB. 2001. Incorporation of a Fault factor into the stability graph method: Kidd mine case studies. Mineral Resour Eng. 10 (01):3–37.

Vallejos JA, Delonca A, Fuenzalida J, Burgos L. 2016. Statistical analysis of the stability number adjustment factors and implications for underground mine design. Int J Rock Mech Min Sci. 87(Supplement C):104–112.

Vallejos JA, Miranda R, Burgos L, Perez E. 2017. Development of new design tools for open stoping underground mines. The 51st US rock mechanics/geomechanics symposium; June 25–28; San Francisco, CA, USA.

Veelenturf LPJ. 1995. Analysis and applications of artificial neural networks. Midsomer Norton: Prentice Hall International (UK) Ltd.

Yang H, Liu J, Zhou X. 2017. Effects of the loading and unloading conditions on the stress relaxation behavior of pre-cracked granite. Rock Mech Rock Eng. 50 (5):1157–1169.